

Simple Diagonal Designs with Reconfigurable Real-Time Circuits

Yizhi Shen,^{1,*} Katherine Klymko,² Eran Rabani,^{3,4,5} Norm M. Tubman,⁶ Daan Camps,² Roel Van Beeumen,¹ and Michael Lindsey⁷

¹*Applied Mathematics and Computational Research Division,
Lawrence Berkeley National Laboratory, Berkeley, CA 94720, USA*

²*NERSC, Lawrence Berkeley National Laboratory, Berkeley, CA 94720, USA*

³*Materials Sciences Division, Lawrence Berkeley National Laboratory, Berkeley, CA 94720, USA*

⁴*Department of Chemistry, University of California, Berkeley, Berkeley, CA 94720, USA*

⁵*The Sackler Center for Computational Molecular and Materials Science, Tel Aviv University, Tel Aviv 69978, Israel*

⁶*NASA Ames Research Center, Moffett Field, CA 94035, USA*

⁷*Department of Mathematics, University of California, Berkeley, Berkeley, CA 94720, USA*

Unitary designs are widely used in quantum computation, but in many practical settings it suffices to construct a diagonal state design generated with unitary gates diagonal in the computational basis. In this work, we introduce a simple and efficient diagonal state design based on real-time evolutions. Our construction is inspired by the classical Girard-Hutchinson trace estimator in that it involves the stochastic preparation of random-phase states. Although the exact Girard-Hutchinson states are not tractably implementable on a quantum computer, we can construct states that match the statistical moments of the Girard-Hutchinson states with real-time evolution. Importantly, our random states are all generated using the same Hamiltonians for real-time evolution, with the randomness arising solely from stochastic variations in the durations of the evolutions. In this sense, the circuit is fully reconfigurable and thus suited for near-term realizations on both digital and analog platforms.

I. INTRODUCTION

Unitary designs, which faithfully reproduce statistical moments of the Haar distribution, play an important role in quantum information science, with wide-ranging applications including channel benchmarking, state or process tomography, and quantum linear algebra [1–4]. For many problems, it suffices to consider the class of diagonal unitary designs, which consist solely of diagonal unitary operations [5, 6]. In principle, constructing a diagonal design should simplify the resulting circuits. Moreover, the restriction to purely diagonal gates augments the feasibility of fault-tolerant, error-corrected implementations [7]. Despite their simplicity, diagonal designs can be highly useful in randomization tasks. Notably, their scrambling properties are sufficient for powerful tomographic probes that predict arbitrary state properties [8–11].

In this manuscript, we introduce a quantum algorithm for constructing a diagonal 3-design, which samples random states within a quantum many-body Hilbert space. To prepare these random states (i.e., wavefunctions), we only make use of real-time evolutions under a fixed set of simple auxiliary Hamiltonians, where only the evolution durations are randomized (and moreover independent of the system size). Due to phase cancellation, the random states yield a stochastic resolution of identity. Since the auxiliary Hamiltonians are fixed and only the evolution durations are randomized, we say that the circuit implementing our diagonal 3-design is *reconfigurable*. That is, on both digital and analog platforms, we construct a single hardware-native circuit designed for reuse over many samples.

Compared to other approaches for constructing state designs, the strengths of our approach are that it (1) generates random states through simple real-time evolutions whose durations can be randomized independently of the system size, (2) exactly attains the desired statistical moments while avoiding expensive handling of exponentially large Hilbert spaces, and (3) significantly enhances practical near-term quantum efficiency, since it eliminates the overhead required for approaches that implement a distinct circuit for each sampling instance.

The manuscript is organized as follows. In Section II, we start with an overview of unitary and diagonal unitary designs, highlighting the connections and disparities. We then expand on the intuition that real-time evolutions of randomized duration can fulfill the conditions of diagonal design. In Section III, we present a practical approach for constructing a diagonal design. We explicitly compute its moments and detail its reconfigurable circuit representations on both digital and analog platforms. In Section IV, we summarize and conclude.

The real-time construction in Section III is well-suited for state tomography. Interestingly, recent ideas based on Hamiltonian-driven shadows [8–11] have demonstrated promising potential due to their native implementations on analog simulators. In particular, real-time evolution following a single random duration (discussed concretely in Section III B) can be employed to generate shadows as considered in the work [11], which assumes access to the ideal random diagonal ensemble. Our work reveals that this ensemble can be sampled using several independent real-time evolutions of tractable duration.

* yizhis@lbl.gov

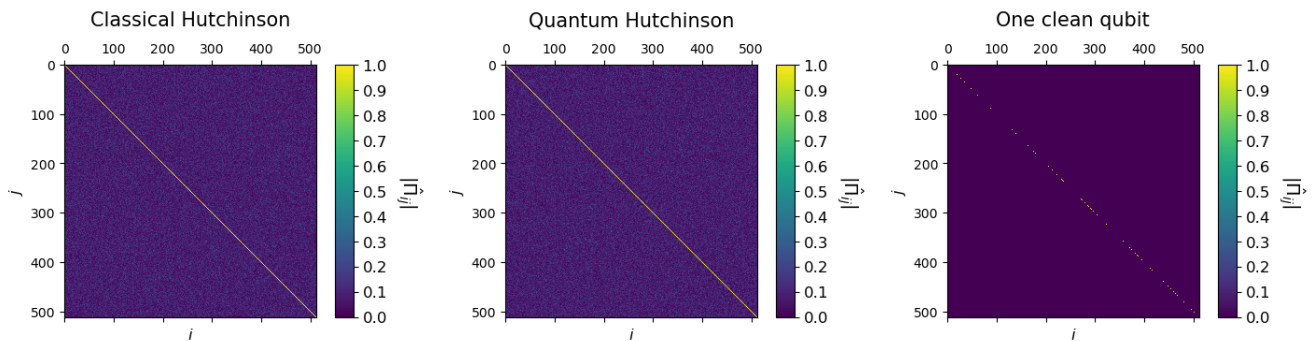


FIG. 1. Approximate resolution of identity $\hat{\Pi} = \frac{N}{K} \sum_{k=1}^K |\chi_k\rangle \langle \chi_k|$ constructed with $K = 10^2$ random states of various types. **Left:** Classical Hutchinson states. **Center:** Quantum Hutchinson states (this work). **Right:** Uniformly sampled computational basis, corresponding to the one clean qubit construction. Matrix elements $\hat{\Pi}_{ij}$ of the approximate identity operator are colored by their magnitudes. Color interpolates linearly from dark blue ($|\hat{\Pi}_{ij}| = 0$) to yellow ($|\hat{\Pi}_{ij}| = 1$).

II. REVIEW OF UNITARY AND DIAGONAL STATE DESIGNS

A unitary design is an ensemble of unitary operators $U \sim p$ drawn according to a distribution p which matches certain statistical moments of the Haar distribution over the unitary group. Specifically, a unitary d -design fulfills the defining property that for any quantum state $|\psi\rangle$,

$$\mathbb{E}_{U \sim p} \left[(U |\psi\rangle \langle \psi| U^\dagger)^{\otimes d} \right] = \mathbb{E}_{U \sim \text{Haar}} \left[(U |\psi\rangle \langle \psi| U^\dagger)^{\otimes d} \right]. \quad (1)$$

The matching property of Eq. (1) is valuable for a variety of tasks due to the prohibitive cost of explicitly sampling a random quantum circuit from the Haar distribution. In contrast, unitary designs offer a more feasible alternative as they are comparatively simpler to construct. [2, 12, 13]

Meanwhile, *diagonal* unitary designs relax the requirement of matching the full Haar randomness. As its name suggests, a diagonal design involves the action of diagonal unitary operators $U \sim p_{\text{diag}}$ on some reference state [5, 6]. To introduce the associated moment-matching property analogous to Eq. (1), we first consider the N -dimensional random-phase state $|\phi\rangle \in \mathbb{C}^N$,

$$|\phi\rangle = \sum_{\vec{n} \in \{0,1\}^Q} \phi_{\vec{n}} |\vec{n}\rangle = \frac{1}{\sqrt{N}} \sum_{\vec{n} \in \{0,1\}^Q} e^{-i\theta_{\vec{n}}} |\vec{n}\rangle, \quad (2)$$

where we allocate $Q = \lceil \log_2 N \rceil$ qubits to store the state, and $\theta_{\vec{n}} \sim \text{Uniform}(0, 2\pi)$ are independent and identically distributed random variables for all computational basis elements \vec{n} . Historically, the use of random-phase vectors $|\phi\rangle$ can be traced back to the seminal work of Girard and Hutchinson on stochastic trace estimation [14–16], for which the coefficients $\phi_{\vec{n}}$ are sampled independently and uniformly from $\{\pm 1\}$, i.e., the Rademacher distribution, on a classical computer. For this reason, throughout our manuscript we refer to the state $|\phi\rangle$ following Eq. (2) as a classical or conventional Hutchinson state. Accordingly,

a diagonal d -design is an ensemble of diagonal unitaries such that for some reference state $|\chi_0\rangle$, it holds that

$$\mathbb{E}_{U \sim p_{\text{diag}}} \left[(U |\chi_0\rangle \langle \chi_0| U^\dagger)^{\otimes d} \right] = \mathbb{E} \left[(|\phi\rangle \langle \phi|)^{\otimes d} \right], \quad (3)$$

where $|\phi\rangle$ on the right-hand side of Eq. (3) is understood to be a conventional Hutchinson state. We comment that it is not tractable to sample wavefunctions with independent components in the computational basis, such as the conventional Hutchinson state.

The matching property prescribed above can be leveraged in computational routines essential for various quantum algorithms. Among the earliest applications is the one clean qubit model of computation [17], a computing paradigm targeting maximally mixed states. In particular, the state $\frac{1}{N} \mathbb{I}$ is stochastically simulated by uniformly sampling the computational basis $\{|\vec{n}\rangle\}_{n=0}^{N-1}$, which forms a 1-design. Moreover, the application of diagonal 2-designs to trace estimation matches the variance yielded by the conventional Hutchinson estimator, which is optimal among all estimators with independent components in the computational basis [16]. The connection between diagonal designs and trace estimation has not been previously observed to our knowledge. In addition, diagonal 3-designs can be exploited to perform accurate state tomography. This capability is crucial for recent Hamiltonian-driven shadows [8–11], which have demonstrated efficient prediction of arbitrary state observables on practical analog simulators.

To construct a state design, typically the scrambling circuits are composed randomly from some suitable pool of candidate gates. For example, the Hadamard, phase, and CNOT gates combinatorially generate the Clifford group as a unitary 2-design, while single-qubit and controlled rotations [5] are sufficient to generate a diagonal unitary 2-design. These approaches hence necessitate the realization of a distinct circuit for each sampled random state. Despite encouraging theoretical guarantees on circuit preparation such as polynomial gate count [5, 6, 18], implementing these designs on near-term hardware would

still be costly, since the generation of each random state requires executing a new circuit compilation with varying gate composition and sequencing.

In our approach, we prioritize minimal quantum resource requirements for constructing a diagonal design. The central ingredient is the real-time evolution of a single, easily-prepared reference state for a random duration of time. Using this ingredient, we can generate random states achieving the matching identities Eq. (3) for $d = 3$. Importantly, our design is reconfigurable in the sense we have described above (as it avoids the repetitive synthesis of scrambling circuits), distinguishing itself from existing approaches. Furthermore, the construction is conceptually simple. We refer to our random states, $|\chi\rangle = U|\chi_0\rangle$, as *quantum Hutchinson states*. To illustrate the different approaches described in this section and to motivate the quantum Hutchinson approach investigated in this work, we present a comparison of classical Hutchinson, quantum Hutchinson, and one clean qubit approaches for the resolution of the identity, as shown in Fig. 1. The figure provides a visualization of how the quantum Hutchinson approach achieves a high-fidelity approximation to the identity compared to the one clean qubit approach with the same number of samples. Additionally, the quantum and classical Hutchinson states produce nearly identical approximations, despite the exponentially higher cost for generating the latter.

III. MAIN RESULTS

A. Quantum Hutchinson state construction

In this section we present the construction of our quantum Hutchinson states.

First we prepare the initial state of our circuit, which is a uniform superposition of the Z -computational basis elements $|\vec{n}\rangle \in \{0, 1\}^Q$:

$$|\chi_0\rangle = |+\rangle^{\otimes Q} = \frac{1}{\sqrt{N}} \sum_{\vec{n} \in \{0, 1\}^Q} |\vec{n}\rangle, \quad (4)$$

with the use of $Q = \log_2 N$ Hadamard gates.

We evolve this initial state under the following diagonal Hamiltonian of spin-glass type:

$$G = \sum_{i \leq j}^Q \gamma_{ij} \Gamma_i \Gamma_j, \quad (5)$$

where $\Gamma_i = \frac{1-Z_i}{2}$ denotes the number operator acting on the qubit i , alternatively defined by $\Gamma_i |\vec{n}\rangle = n_i |\vec{n}\rangle$, and $\gamma_{ij} \sim \text{Uniform}(0, 2\pi)$ are independent and identically

distributed random variables for all pairs of qubits $i \leq j$. We will evolve under G for one unit of time, and this action can be viewed as a sequence of real-time evolutions by all of the $\Gamma_i \Gamma_j$ (which all commute and hence do not introduce any Trotter error) for respective durations γ_{ij} . The quantum Hutchinson states are therefore sampled as

$$|\chi\rangle = e^{-iG} |\chi_0\rangle = \prod_{i \leq j}^Q e^{-i\gamma_{ij} \Gamma_i \Gamma_j} |\chi_0\rangle. \quad (6)$$

B. Construction with a single random time

As a theoretical question, it is interesting to consider whether it is possible to construct a suitable quantum Hutchinson state as $|\chi\rangle = e^{-iGt} |\chi_0\rangle$, where G is a single fixed Hamiltonian and t is a single random time. In fact, as we show in Appendix A, it is possible to achieve this goal where G is taken to be a linear combination of the diagonal operators Γ_i and $\Gamma_i \Gamma_j$. However, the random time t must be exponentially long in the number of qubits Q . Ultimately it is convenient to view such a long real-time evolution as a sequence of individual real-time evolutions, whose durations are drawn from a different joint distribution than that of our main construction, according to the Hamiltonian components Γ_i and $\Gamma_i \Gamma_j$. From this point of view, the construction Eq. (6) emerges as a simpler alternative in which all the short random times are drawn independently. Moreover, the construction Eq. (6) enjoys the same hardware advantages of real-time evolution under a fixed set of elementary two-qubit Hamiltonians. Nonetheless, due to potential theoretical interest, we give further detail on the single-time construction in Appendix A, and we comment that in fact this work was initially motivated by this perspective.

C. Statistical properties

Now we show that the quantum Hutchinson state constructed in Eq. (6) is a diagonal 3-design.

Theorem 1. Consider the quantum Hutchinson and conventional Hutchinson states drawn randomly according to Eq. (6) and Eq. (2), respectively. The moments of these two constructions match up to third order in the sense that, for $d \leq 3$,

$$\mathbb{E} \left[(|\chi\rangle \langle \chi|)^{\otimes d} \right] = \mathbb{E} \left[(|\phi\rangle \langle \phi|)^{\otimes d} \right]. \quad (7)$$

Proof. We first observe that the Hutchinson construction admits the statistical moments

$$\mathbb{E} \left[(|\phi\rangle\langle\phi|)^{\otimes 1} \right] = \frac{1}{N} \sum_{\vec{n}} |\vec{n}\rangle \langle\vec{n}|, \quad (8)$$

$$\mathbb{E} \left[(|\phi\rangle\langle\phi|)^{\otimes 2} \right] = \frac{1}{N^2} \sum_{\substack{\vec{m}, \vec{m}', \vec{n}, \vec{n}': \\ (\vec{m}, \vec{m}') = \mathcal{P}_2(\vec{n}, \vec{n}') \text{ for some } \mathcal{P}_2 \in S_2}} |\vec{m}\vec{m}'\rangle \langle\vec{n}\vec{n}'|, \quad (9)$$

$$\mathbb{E} \left[(|\phi\rangle\langle\phi|)^{\otimes 3} \right] = \frac{1}{N^3} \sum_{\substack{\vec{m}, \vec{m}', \vec{m}'', \vec{n}, \vec{n}', \vec{n}'': \\ (\vec{m}, \vec{m}', \vec{m}'') = \mathcal{P}_3(\vec{n}, \vec{n}', \vec{n}'') \text{ for some } \mathcal{P}_3 \in S_3}} |\vec{m}\vec{m}'\vec{m}''\rangle \langle\vec{n}\vec{n}'\vec{n}''|, \quad (10)$$

where the $\mathcal{P}_d \in S_d$ appearing in the summations above indicate permutations of d binary vectors. The vector equality constraints up to permutation arise from the statistical independence of random phases $\theta_{\vec{n}}$ in Eq. (6).

Next we consider the quantum Hutchinson construction. Note that if $\gamma \sim \text{Uniform}(0, 2\pi)$, then for any integer k , the expectation $\mathbb{E}[e^{ik\gamma}]$ is one if $k = 0$ and zero otherwise. This identity enables the computations:

$$\mathbb{E} \left[(|\chi\rangle\langle\chi|)^{\otimes 1} \right] = \frac{1}{N} \sum_{\vec{m}, \vec{n}} \prod_{i \leq j}^Q \mathbb{E} [e^{i(n_i n_j - m_i m_j) \gamma}] |\vec{m}\rangle \langle\vec{n}|, \quad (11)$$

$$= \frac{1}{N} \sum_{\vec{m}, \vec{n}} \prod_{i \leq j}^Q \delta_{n_i n_j, m_i m_j} |\vec{m}\rangle \langle\vec{n}|, \quad (12)$$

$$= \frac{1}{N} \sum_{\substack{\vec{m}, \vec{n}: \\ \vec{m} \otimes \vec{m} = \vec{n} \otimes \vec{n}}} |\vec{m}\rangle \langle\vec{n}| \stackrel{\text{(Lemma 1)}}{=} \mathbb{E} \left[(|\phi\rangle\langle\phi|)^{\otimes 1} \right], \quad (13)$$

$$\mathbb{E} \left[(|\chi\rangle\langle\chi|)^{\otimes 2} \right] = \frac{1}{N^2} \sum_{\vec{m}, \vec{m}', \vec{n}, \vec{n}'} \prod_{i \leq j}^Q \delta_{n_i n_j + n'_i n'_j, m_i m_j + m'_i m'_j} |\vec{m}\vec{m}'\rangle \langle\vec{n}\vec{n}'|, \quad (14)$$

$$= \frac{1}{N^2} \sum_{\substack{\vec{m}, \vec{m}', \vec{n}, \vec{n}': \\ \vec{m} \otimes \vec{m} + \vec{m}' \otimes \vec{m}' = \vec{n} \otimes \vec{n} + \vec{n}' \otimes \vec{n}'}} |\vec{m}\vec{m}'\rangle \langle\vec{n}\vec{n}'| \stackrel{\text{(Lemma 1)}}{=} \mathbb{E} \left[(|\phi\rangle\langle\phi|)^{\otimes 2} \right], \quad (15)$$

$$\mathbb{E} \left[(|\chi\rangle\langle\chi|)^{\otimes 3} \right] = \frac{1}{N^3} \sum_{\substack{\vec{m}, \vec{m}', \vec{m}'', \vec{n}, \vec{n}', \vec{n}'': \\ \vec{m} \otimes \vec{m} + \vec{m}' \otimes \vec{m}' + \vec{m}'' \otimes \vec{m}'' = \vec{n} \otimes \vec{n} + \vec{n}' \otimes \vec{n}' + \vec{n}'' \otimes \vec{n}''}} |\vec{m}\vec{m}'\vec{m}''\rangle \langle\vec{n}\vec{n}'\vec{n}''| \stackrel{\text{(Lemma 1)}}{=} \mathbb{E} \left[(|\phi\rangle\langle\phi|)^{\otimes 3} \right]. \quad (16)$$

To arrive at Eqs. (13), (15) and (16) in the calculations, we have used the following lemma:

Lemma 1. For vectors $\vec{m}_1, \vec{m}_2, \vec{m}_3, \vec{n}_1, \vec{n}_2, \vec{n}_3 \in \{0, 1\}^Q$ and integer $1 \leq d \leq 3$, the matrix identity,

$$\sum_{i=1}^d \vec{m}_i \otimes \vec{m}_i = \sum_{i=1}^d \vec{n}_i \otimes \vec{n}_i, \quad (17)$$

holds if and only if $(\vec{m}_1, \dots, \vec{m}_d) = \mathcal{P}_d(\vec{n}_1, \dots, \vec{n}_d)$ for some permutation $\mathcal{P}_d \in S_d$. Here \otimes is understood as the vector outer product.

The proof of Lemma 1 is presented in Appendix B. This completes the proof of Theorem 1. \square

Now let us illustrate how Theorem 1 is applied to yield guarantees on our random states $|\chi\rangle$. First, the base case $d = 1$, together with Eq. (8), establishes the stochastic resolution of identity, $\mathbb{E} [|\chi\rangle\langle\chi|] = \frac{1}{N} \mathbb{I}$, essential in many randomization tasks. Second, we examine the case $d = 2$. Theorem 1 in this case, combined with Eq. (9), implies that

$$\mathbb{E} \left[(|\chi\rangle\langle\chi|)^{\otimes 2} \right] = \left(\frac{1}{N} \sum_{\vec{n}} |\vec{n}\rangle \langle\vec{n}| \right)^{\otimes 2} + \frac{1}{N^2} \sum_{\vec{m} \neq \vec{n}} |\vec{m}\vec{n}\rangle \langle\vec{n}\vec{m}|, \quad (18)$$

recovering the well-known second moment of conven-

tional Hutchinson states:

$$\mathbb{E} \left[|\langle \chi | A | \chi \rangle|^2 \right] = |\mathbb{E} \langle \chi | A | \chi \rangle|^2 + \frac{1}{N^2} \sum_{\vec{m} \neq \vec{n}} |\langle \vec{m} | A | \vec{n} \rangle|^2, \quad (19)$$

where $A \in \mathbb{C}^{N \times N}$ and $\mathbb{E} \langle \chi | A | \chi \rangle = \frac{1}{N} \text{Tr}[A]$.

Alternatively we can express the variance as

$$\mathbb{V} [\langle \chi | A | \chi \rangle] = \frac{1}{N^2} \sum_{\vec{m} \neq \vec{n}} |\langle \vec{m} | A | \vec{n} \rangle|^2 \leq \frac{1}{N^2} \|A\|_F^2, \quad (20)$$

where we have a succinct bound in terms of the Frobenius norm of the operator A . Note that the exact expression for the variance can often be reduced through a similarity transformation, for example if A enjoys certain symmetries [19]. By Chebyshev's inequality, taking an empirical average over K randomly sampled states, we expect that with high probability

$$\left| \frac{1}{K} \sum_{k=1}^K \langle \chi_k | A | \chi_k \rangle - \frac{1}{N} \text{Tr}[A] \right| \leq \frac{1}{N} \|A\|_F \epsilon, \quad (21)$$

where $\epsilon = \mathcal{O}(\frac{1}{\sqrt{K}})$ independently of A . In this sense, we say that the fluctuations of the estimator for the normalized operator trace are on the order of $\frac{1}{N} \|A\|_F$.

D. Reconfigurability on digital platforms

Next we examine the hardware requirements for our diagonal 3-design on a digital quantum platform. In particular, all quantum Hutchinson instances can be realized with a single reconfigurable quantum circuit.

Observe that by using $\Gamma_i \Gamma_j = \frac{1}{4}(1 - Z_i - Z_j + Z_i Z_j)$, the Hamiltonian G from Eq. (5) can be rewritten, up to a global phase, in terms of the Pauli Z operators as the Ising-type Hamiltonian,

$$G = \sum_{i < j}^Q h_{ij} Z_i Z_j + \sum_{i=1}^Q h_i Z_i, \quad (22)$$

with the Ising couplings and external field strengths given by $h_{ij} = \frac{\gamma_{ij}}{4}$ and $h_i = -\frac{\gamma_{ii}}{2} - \sum_{j>i} \frac{\gamma_{ij}}{4}$. The unitary time evolution in the Z -basis is hence a product of elementary diagonal gates,

$$e^{-iGt} = \left(\prod_{i \neq j}^Q e^{-ih_{ij} Z_i Z_j t} \right) \left(\prod_{i=1}^Q e^{-ih_i Z_i t} \right), \quad (23)$$

$$= \left(\prod_{i < j}^Q R_{zz}(4h_{ij}t|i, j) \right) \left(\bigotimes_{i=1}^Q R_z(2h_i t|i) \right), \quad (24)$$

where $R_z(\phi|i)$ and $R_{zz}(\phi|i, j)$ are one- and two-qubit Z -rotations of angle ϕ respectively. Each two-qubit rotation

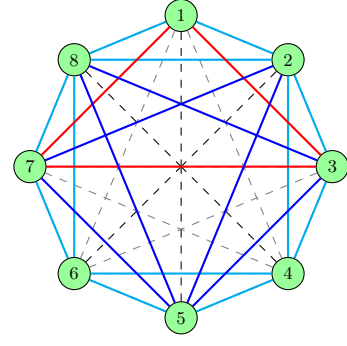


FIG. 2. Edge-disjoint triangles in a complete graph with $|\mathcal{V}| = Q = 8$ vertices. The colors distinguish triangles with different connectivities.

can be further unfolded as a CNOT-conjugated one-qubit rotation,

$$R_{zz}(\phi|i, j) = C_x(i, j) R_z(\phi|j) C_x(i, j), \quad (25)$$

where the CNOT, $C_x(i, j)$, acts on the control and target qubits (i, j) . Hence, the circuit can be efficiently synthesized using only one-qubit Z -rotations and two-qubit CNOT gates.

Notably, the quantum Hutchinson state sampling only involves modification of the $\mathcal{O}(Q^2)$ rotation angles but does not involve replacement or reordering of any gates. Moreover, by exploiting gate commutation relations, we can bound both the gate count and circuit depth required to produce a quantum Hutchinson state (cf. Theorem 2 below). The circuit we have presented yields a naïve gate count scaling of $\mathcal{O}(Q^2)$, with $\frac{Q(Q+1)}{2} R_z$ gates and $Q(Q-1)$ CNOT gates. While the implementation of this circuit is indeed feasible on devices with native all-to-all connectivity, we can slightly improve the naïve gate count and moreover show that the circuit depth is $\mathcal{O}(Q)$.

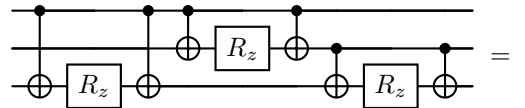
Theorem 2. e^{-iG} can be implemented using a single circuit with depth no greater than $D = 9Q - 2$, where the circuit contains $\frac{Q(Q+1)}{2} R_z$ gates and at most $N_{\text{CNOT}} = \lfloor \frac{5Q^2 - 3Q - 2}{6} \rfloor$ CNOT gates.

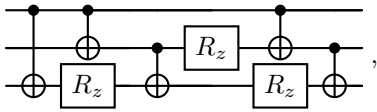
Proof. We exploit the commutation or rewriting rules for R_z and CNOT gates,

$$C_x(j, k) R_{zz}(\phi|i, j) = R_{zz}(\phi|i, j) C_x(j, k), \quad (26)$$

$$C_x(i, j) C_x(j, k) C_x(i, k) = C_x(j, k) C_x(i, j), \quad (27)$$

where (i, j, k) indexes a triplet of distinct qubit registries. When combined, the rules help improve local compilation as illustrated graphically below,





resulting in a reduction in both the gate count and circuit depth for a three-qubit block. Recall that each $R_{zz}(\phi|i, j)$ uniquely captures a two-body interaction $h_{ij}Z_iZ_j$ in G . So the overall resource reduction from our improved local compilation can be estimated by identifying the triplets or triangles (i, j, k) that lack shared edges in an all-to-all graph representing our Ising Hamiltonian. This is a topic deeply examined in graph theory and combinatorics [20–22]. In particular, we highlight the fact that in a complete graph, $\mathcal{G} = (\mathcal{V}, \mathcal{E})$ with $|\mathcal{E}| = \frac{|\mathcal{V}|(|\mathcal{V}|-1)}{2}$, the maximal number of such edge-disjoint triangles is at least $N_a \geq \frac{(|\mathcal{V}|-1)(|\mathcal{V}|-2)}{6}$. For example, Fig. 2 shows the assembly of different three-qubit blocks in a 8-qubit complete graph, where a set of 7 edge-disjoint triangles is highlighted. The number of ‘dangling’ edges untouched by the triangles is therefore bounded by $N_b \leq |\mathcal{E}| - 3N_a = Q - 1$, which gives a total CNOT count of

$$N_{\text{CNOT}} \leq 5N_a + 2N_b. \quad (28)$$

Moreover, it is apparent that any two triangles commute with each other unless they share a common vertex. This observation allows us to bound the circuit depth,

$$D \leq 12 \lfloor \frac{Q}{2} \rfloor + 3N_b + 1, \quad (29)$$

where the first two terms in Eq. (29) account for the $\lfloor \frac{Q}{2} \rfloor$ layers of triangles with varying connectivities, as marked by the different colors in Fig. 2, and N_b layers of untouched dangling edges. We also include the layer of R_z gates that capture the external fields $\{h_i Z_i\}_{i=1}^Q$ in G .

(For the special cases $Q \equiv 1 \pmod{6}$ or $Q \equiv 3 \pmod{6}$, we saturate the optimal number of edge-disjoint triangles, $N_a = \frac{Q(Q-1)}{6}$. This implies a tighter bound of $N_{\text{CNOT}} \leq \frac{5Q^2-5Q}{6}$ and $D \leq 6Q + 1$ in these cases.) \square

E. Reconfigurability on analog platforms

In this section, we proceed to investigate the hardware implementation of our diagonal 3-design on a dynamics-driven analog platform, where the construction based on the real-time evolution yields significant advantages. Our analysis primarily centers around systems of interacting neutral atoms undergoing Rydberg excitations [23, 24]. Although our focus is specific, similar considerations can hold for other analog models.

Recall that a general Rydberg Hamiltonian takes the form

$$G_{\text{Rydberg}} = \sum_{i=1}^Q \Omega_i X_i + \sum_{i=1}^Q \Delta_i \Gamma_i + \sum_{i<j}^Q V_{ij} \Gamma_i \Gamma_j, \quad (30)$$

where Ω_i and Δ_i determine the local Rabi frequency and detuning, respectively, on the atomic site i , while $V_{ij} \propto \frac{1}{r_{ij}^6}$ sets the repulsive van der Waals interaction between sites i and j separated by a distance of r_{ij} . Therefore our spin-glass Hamiltonian G is natively Rydberg with vanishing Rabi driving, $\Omega_i \equiv 0$.

In addition, preparation of the initial state can be accomplished by unit-time evolution under another Rydberg Hamiltonian of the form of Eq. (30), where $\Omega_i = -\frac{\Delta_i}{2} = -\frac{\pi}{2\sqrt{2}}$ and $V_{ij} \equiv 0$. This is the case because

$$|\chi_0\rangle = \bigotimes_{i=1}^Q e^{i\frac{\pi}{2\sqrt{2}}(X_i+Z_i)} |\vec{0}\rangle, \quad (31)$$

where physical ground state $|\vec{0}\rangle$ is the native atomic configuration.

The overall evolution that we require, including the preparation of $|\chi_0\rangle$ can therefore be produced using the time-dependent waveforms,

$$\begin{cases} (\Omega_i, \Delta_i) = (-\frac{\pi}{2\sqrt{2}}, \frac{\pi}{\sqrt{2}}), & 0 \leq t \leq 1 \\ (\Omega_i, \Delta_i) = (0, \gamma_{ii}), & 1 \leq t \leq 2 \end{cases}, \quad (32)$$

prescribing piecewise-constant local Rabi drivings as well as detunings.

Moving forward, we discuss the simulation of the remaining pairwise coupling terms with physical interactions V_{ij} . Naively, given positive weights $\gamma_{ij} \stackrel{\text{iid}}{\sim} \text{Uniform}(0, 2\pi)$, we must choose the Q atomic positions \vec{r}_i so that the resulting distances $r_{ij} = \|\vec{r}_i - \vec{r}_j\|_2$ satisfy $V_{ij}(r_{ij}) = \gamma_{ij}$. However, this embedding problem is NP-hard when Q exceeds the spatial dimension (which is 3 at most), and valid solution does not exist in most cases.

Instead we formulate an alternative approach by exploiting the commutation of the diagonal operators Γ_i . As a first attempt we consider the decomposition $e^{-iGt} = \prod_{i<j} e^{-iG_{ij}t}$ where

$$G_{ij} := \gamma_{ij} \Gamma_i \Gamma_j + \frac{1}{Q-1} (\gamma_{ii} \Gamma_i + \gamma_{jj} \Gamma_j), \quad (33)$$

which holds because $\Gamma_i = \Gamma_i \Gamma_i$ for each i . The regrouping of the Hamiltonian contributions suggests that we should achieve the analog evolution e^{-iGt} using $\frac{Q(Q-1)}{2}$ analog blocks $e^{-iG_{ij}t}$ each of which couples only a single pair of atoms, and between which atom positions are dynamically shuffled.

However, by considering a more sophisticated coupling within each analog block we can bring the block depth down to Q . Theorem 3 below states this result and moreover quantifies the atom shuffling that we require between blocks in terms of the number of SWAP gates, each of which is realized as the physical swapping of a pair of atoms. In this construction, it is more convenient to work with simplified γ_{ij} that are sampled i.i.d. from the uniform distribution over the discrete set $\{0, \frac{2\pi}{3}, \frac{4\pi}{3}\}$. If γ is so distributed, then for any integer k , the expectation

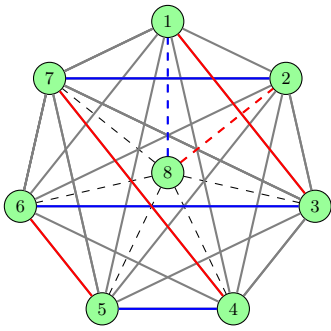


FIG. 3. Edge-coloring of a complete graph with $|\mathcal{V}| = Q = 8$ vertices. The colors partition all the edges into $(Q-1)$ groups. Each group represents a unique atom configuration consisting of disjoint doublets. For purpose of visualization, we highlight two of the colored groups (red and blue respectively).

$\mathbb{E}[e^{ik\gamma}]$ is one if k is an integer multiple of 3 and zero otherwise. Therefore the variance equality from Theorem 1 holds just as well in this case.

Theorem 3. e^{-iG} can be implemented on a Rydberg simulator with at most Q analog blocks. Each of these analog blocks performs Rydberg evolution of time $\mathcal{O}(1)$ for a one-dimensional chain of Q Rydberg atoms. The circuit also involves a total of at most $N_{\text{SWAP}} = \frac{Q(Q-1)}{2}$ SWAP gates, i.e., the physical swaps of two atoms, which appear in between the analog blocks.

Proof. The use of the discrete couplings γ_{ij} allows us to consider only three physical distances $r_2 < r_1 < r_0$ such that $V_{ij}(r_2) = \frac{4\pi}{3}$, $V_{ij}(r_1) = \frac{2\pi}{3}$, and $V_{ij}(r_0) = 0$. This choice is possible owing to the rapid decay of the van der Waals interaction.

We now invoke classic edge coloring results for a complete graph of Q vertices corresponding to the Q qubits. Specifically, the edges of this graph can be decorated with at most Q different colors so that no incident edges have the same color. In general, edge colorings can be assigned efficiently with $\mathcal{O}(\text{poly}(Q))$ runtime [25, 26], but we make use of a very specific construction for the complete graph.

Without loss of generality, we assume that Q is even and use the following coloring. We distribute $Q-1$ vertices evenly on a circle to create a regular polygon and locate the remaining vertex at the center of the circle, as illustrated in Fig. 3. Then we assign a distinct color to each edge connecting a central-exterior vertex pair (as indicated by dashed lines in Fig. 3), and color the edges perpendicular to the central edge (as solid lines in Fig. 3). This assignment uses $\frac{|\mathcal{E}|}{|\mathcal{V}|/2} = Q-1$ colors to cover our complete graph.

Let $\{\mathcal{E}_i\}_{i=1}^{Q-1}$ be a partition of the edge set \mathcal{E} ,

$$\bigsqcup_{i=1}^{Q-1} \mathcal{E}_i = \mathcal{E}, \quad (34)$$

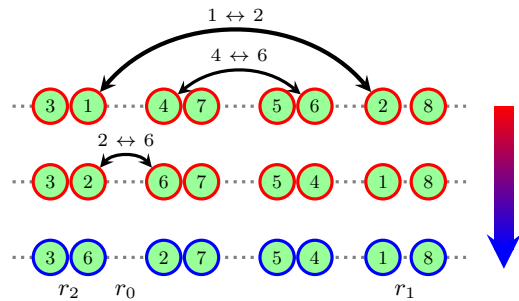


FIG. 4. Embedding of the edge-colored graph onto a 1D chain of interacting neutral atoms with $|\mathcal{V}| = Q = 8$ qubits. Each color, assigned on a subset of $Q/2$ edges, designates a dimer pairing of the vertices, which is reconfigured after each analog block e^{-iG_k} . The swapping involved in one such dimer reconfiguration (red to blue as in Fig. 3) is illustrated from top to bottom. The black bent arrows indicate the sequence of vertex transpositions needed to transition from the old to the new color assignment.

resulting from the coloring scheme above. Our analog evolution can thus be achieved using $Q-1$ blocks,

$$e^{-iG} = \prod_{k=1}^{Q-1} e^{-iG_k} = \prod_{k=1}^{Q-1} \prod_{(i,j) \in \mathcal{E}_k} e^{-iG_{ij}}, \quad (35)$$

where the Hamiltonian G_k for each analog block only includes interactions between atom dimers that share the same color assignment. The block Hamiltonian G_k can be embedded onto a one-dimensional lattice with variable lattice spacing r_0 , r_1 and r_2 as sketched in Fig. 4. To change the dimer configuration from G_k to G_{k+1} , we permute $Q/2$ vertices on the lattice since we can redistribute them to pair with the remaining half of the vertices. For example, the pairing $(3,1) \mapsto (3,6)$ in Fig. 4 from red to blue leaves the vertex 3 untouched. Such a permutation can be written as a sequence of at most $\frac{Q}{2} - 1$ elementary transpositions. A transposition of the two vertices i and j corresponds to the physical swapping of two atom positions. Such atom swaps upon the application of each analog block are shown schematically in Fig. 4. We notice that each set of $\frac{Q}{2}$ distinctly colored edges can be associated with one of the exterior edges $(1,2), (2,3), \dots$, etc. Since our graph of polygon exhibits a discrete rotational symmetry along its exterior edges, all the $|\mathcal{V}|$ edges can be decorated as we cycle through the exterior edges. Accordingly, we employ a total of $Q-1$ different permutations throughout the whole analog evolution.

Finally, we remark that the complementary case of odd Q can be adapted readily from the even case, if we introduce an additional, auxiliary vertex to the graph. Combining the two cases, we thereby need at most $N_{\text{SWAP}} = Q(\frac{Q+1}{2} - 1) = \frac{Q(Q-1)}{2}$ to bridge the Q analog blocks. \square

Meanwhile, analog devices with local qubit connectivities, commonly a nearest-neighbor topology, are also ca-

pable of simulating e^{-iG} with a similar resource cost. For nearest-neighbor devices, the identification of the graph Hamiltonian paths [27, 28], for example, enables us to decompose the evolution into $\mathcal{O}(Q)$ analog blocks [29].

IV. CONCLUSION

In this work, we introduce a real-time diagonal design that is efficiently implementable on near-term hardware. Leveraging time evolution under Ising-type Hamiltonians that can be conveniently realized on the digital or analog quantum platforms, we construct randomized ‘quantum Hutchinson’ states. We show that our quantum Hutchinson states match the moments that would be achieved by conventional Hutchinson states in an exponentially high-dimensional space, though the latter can not be efficiently realized with quantum resources. Furthermore, we discuss how to implement the real-time states using a single reconfigurable circuit, whose compilation across different stochastic runs remains unchanged up to the durations of the real-time evolutions. The hardware-adapted implementation suits state-of-the-art digital and analog platforms.

V. ACKNOWLEDGMENTS

This work was funded by the U.S. Department of Energy (DOE) under Contract No. DE-AC0205CH11231, through the Office of Science, Office of Advanced Scientific Computing Research (ASCR) Exploratory Research for Extreme-Scale Science (YS, KK, DC, RVB). This research used resources of the National Energy Research Scientific Computing Center (NERSC), a U.S. Department of Energy Office of Science User Facility located at Lawrence Berkeley National Laboratory, operated under Contract No. DE-AC02-05CH11231. ER acknowledges support from the Center for Computational Study of Excited-State Phenomena in Energy Materials (C2SEPEM) at the Lawrence Berkeley National Laboratory, which is funded by the U.S. Department of Energy, Office of Science, Basic Energy Sciences, Materials Sciences and Engineering Division, under Contract No. DE-AC02-05CH11231, as part of the Computational Materials Sciences Program. NMT is grateful for support from NASA Ames Research Center. This material is based upon work supported by the U.S. Department of Energy, Office of Science, National Quantum Information Science Research Centers, Superconducting Quantum Materials and Systems Center (SQMS) under the contract No. DE-AC02-07CH11359.

APPENDIX

Appendix A: Construction with a single random time

Here we detail the construction, indicated in Section III B, achieving a suitable quantum Hutchinson state with a single random time and a fixed Hamiltonian G .

First, for arbitrary G , consider the full spectral decomposition

$$G = \sum_{n=0}^{N-1} \lambda_n |n^G\rangle \langle n^G|, \quad (\text{A1})$$

with eigenpairs $(\lambda_n, |n^G\rangle)_{n=0}^{N-1}$.

Let us examine the dynamics on an initial state which is a uniform superposition in the G -basis, namely $|\chi^G\rangle := \frac{1}{\sqrt{N}} \sum_{n=0}^{N-1} |n^G\rangle$. For a time $t \in \mathbb{R}$, we denote the corresponding time-evolved state by $|\chi(t)\rangle = e^{-iGt} |\chi^G\rangle$. We will view $|\chi(t)\rangle$ as a random state by randomly sampling *only* the time t from a suitable scalar distribution with probability density $p(t)$. Taking an expectation \mathbb{E} over the time randomness, we arrive at the operator identity,

$$\mathbb{E} [|\chi(t)\rangle \langle \chi(t)|] = \frac{1}{N} \sum_{n,m=0}^{N-1} \mathbb{E} [e^{i(\lambda_n - \lambda_m)t}] |m^G\rangle \langle n^G|, \quad (\text{A2})$$

$$= \frac{1}{N} (\mathbb{I} + \mathbb{B}), \quad (\text{A3})$$

where the operator \mathbb{B} is a bias in the resolution of identity, which we will show can be made zero or extremely small. (Note that in our main construction of Eq. (6), the resolution of identity is always exactly unbiased.)

In the G -basis, \mathbb{B} takes the form,

$$\mathbb{B} = \sum_{n \neq m}^{N-1} \varphi_t(\Delta_{mn}) |m^G\rangle \langle n^G|, \quad (\text{A4})$$

where $\Delta_{mn} = \lambda_n - \lambda_m$ denote the G -eigenvalue differences and $\varphi_t(s) := \mathbb{E}[e^{ist}]$ denotes the characteristic function of the distribution $p(t)$.

A suitable choice of $p(t)$ can effectively control the bias. For example, a Gaussian distribution $p(t) = \frac{1}{\sqrt{2\pi\sigma^2}} e^{-t^2/2\sigma^2}$ yields $\varphi_t(\Delta_{mn}) = e^{-\Delta_{mn}^2\sigma^2/2}$. As σ increases, the bias gets exponentially suppressed. Alternatively, the bias from the fat-tailed distribution $p(t) = \frac{1}{\pi t^2/\sigma} \sin^2(t/\sigma)$ completely vanishes for large σ . In either case, we observe from Eq. (A4) that a nondegenerate G -spectrum, *i.e.*, in which $\Delta_{mn} \neq 0$ for all $m \neq n$, is essential to approximately fulfill the stochastic resolution of identity bias, since indeed $\varphi_t(0) = 1$ always.

In addition to guaranteeing the stochastic resolution of identity, we also want our Hutchinson-type estimator to have an ideal variance. Then for a given operator A

whose trace we seek, we can compute the variance of our estimator as:

$$\mathbb{V}[\langle \chi(t) | A | \chi(t) \rangle] = \sum_{m \neq n} \sum_{m' \neq n'} A_{mn}^* A_{m'n'} \varphi_t(\Delta_{m'n'}^{mn}) \quad (\text{A5})$$

where again the expectation is taken with respect to the distribution $p(t)$ for t and A_{mn} are the matrix elements of A in the G -basis. This variance will match the idealized Hutchinson variance,

$$\sum_{m \neq n} |A_{mn}|^2, \quad (\text{A6})$$

if all the nontrivial differences of eigenvalue differences, denoted $\Delta_{m'n'}^{mn} = \Delta_{mn} - \Delta_{m'n'}$, where $(m, n) \neq (m', n')$ and $(m, m') \neq (n, n')$, are nonzero and the characteristic function is suitably constructed as outlined above.

To make things more concrete, we consider G which is diagonal in the Z -basis, so $|\chi_0\rangle = |\chi^G\rangle = |+\rangle^{\otimes Q}$. As a first attempt, we use the operator G_1 with an equispaced spectrum $\lambda_n = n$, where $n = 0, \dots, N-1$. In fact G_1 can be tractably constructed on the quantum computer with $Q = \log_2 N$ qubits in terms of the one-qubit number operators as

$$G_1 = \sum_{k=1}^Q 2^{k-1} \Gamma_k. \quad (\text{A7})$$

Although the spectrum of G_1 is nondegenerate, the differences of eigenvalue differences are highly degenerate, hence the variance of the resulting Hutchinson-type estimator is severely suboptimal.

In order to recover performance of the classic Hutchinson estimator, we are motivated to ask: can we find a simple parametric form of the G -spectrum $\{\lambda_n\}$ such that the resulting ‘excitations’ $\{\Delta_{mn}\}_{m \neq n}$, are all distinct from one another? This same question motivates the theory of Golomb rulers in number theory [30–32].

The simplest explicit specification of a Golomb ruler is the sequence,

$$\lambda_n = Nn^2 + n, \quad 0 \leq n \leq N-1, \quad (\text{A8})$$

where $\min_{m \neq n} |\Delta_{mn}| = \Delta_{01} = N+1$. It is convenient to normalize our sequence of G -eigenvalues, $\lambda_n = \frac{N}{N+1}n^2 + \frac{1}{N+1}n$, so that the minimal excitation is one: $\min_{m \neq n} |\Delta_{mn}| = 1$.

We can construct a Hamiltonian G_2 achieving this spectrum in terms of G_1 :

$$G_2 = \frac{N}{N+1} G_1^2 + \frac{1}{N+1} G_1, \quad (\text{A9})$$

$$= \sum_{i \neq j}^Q h_{ij} Z_i Z_j + \sum_{i=1}^Q h_i Z_i + \text{const.}, \quad (\text{A10})$$

for suitably defined Ising-type interactions h_{ij} and field strengths h_i .

For an appropriate choice of time randomness, *e.g.*, $p(t) = \frac{1}{\pi t^2/\sigma} \sin^2(t/\sigma)$ with $\sigma > 1$, the exact variance of the conventional Hutchinson estimator is therefore recovered.

Note, however, that the parameters h_{ij} and h_i are exponentially large in the number Q of qubits. In order to construct gates implementing time evolution by G of duration t for a random time $t \sim p(t)$, we would need to compute th_{ij} and th_i modulo 2π to high precision. This is in principle possible but would require extended-precision arithmetic as the number of qubits grows. Since time evolution by G would best be achieved by running separate time evolutions by the component terms of the Hamiltonian (whose durations are only significant modulo 2π), we recover an approach similar to our main construction Eq. (6). Although the simplicity of the construction Eq. (6) is to be preferred, it is interesting to observe the connection.

Appendix B: Proof of Lemma 1

Proof. We first note that the matrix identity,

$$\sum_{i=1}^d \vec{m}_i \otimes \vec{m}_i = \sum_{i=1}^d \vec{n}_i \otimes \vec{n}_i, \quad (\text{B1})$$

implies the vector identity,

$$\sum_{i=1}^d \vec{m}_i = \sum_{i=1}^d \vec{n}_i, \quad (\text{B2})$$

when restricted to the diagonal. Therefore in the $d = 1$ case, $\vec{m}_1 = \vec{n}_1$ holds trivially from Eq. (B2).

For the case $d = 2$, we make the following observation based on Eq. (B2): if $\vec{m}_1 = \vec{n}_1$, it must follow that $\vec{m}_2 = \vec{n}_2$. Therefore we can assume that $\vec{m}_1 \neq \vec{n}_1$, and it remains only to show that $\vec{m}_1 = \vec{n}_2$ or $\vec{n}_1 = \vec{m}_2$, because then in either case Eq. (B2) then immediately implies $(\vec{m}_1, \vec{m}_2) = (\vec{n}_2, \vec{n}_1)$.

By the assumption $\vec{m}_1 \neq \vec{n}_1$, there exists an index $a \in \{1, \dots, Q\}$ such that either $(m_{1,a}, n_{1,a}) = (0, 1)$ or $(m_{1,a}, n_{1,a}) = (1, 0)$. In these respective cases, Eq. (B2) implies the component identity $(m_{2,a}, n_{2,a}) = (1, 0)$ or $(m_{2,a}, n_{2,a}) = (0, 1)$, respectively. Taking the a -th column of Eq. (B1), we obtain

$$m_{1,a} \vec{m}_1 + m_{2,a} \vec{m}_2 = n_{1,a} \vec{n}_1 + n_{2,a} \vec{n}_2. \quad (\text{B3})$$

Therefore we must have either $\vec{n}_1 = \vec{m}_2$ or $\vec{m}_1 = \vec{n}_2$, as was to be shown.

Finally we turn to the case $d = 3$, where we can apply our previous results inductively. First observe that if $\vec{m}_1 = \vec{n}_1$, then by Eq. (B1) and our proof in the case $d = 2$, it follows that $(\vec{m}_2, \vec{m}_3) = \mathcal{P}_2(\vec{n}_2, \vec{n}_3)$ for a suitable permutation \mathcal{P}_2 .

Therefore we can assume that $\vec{m}_1 \neq \vec{n}_1$, so there exists $a \in \{1, \dots, Q\}$ such that $(m_{1,a}, n_{1,a}) = (0, 1)$ or $(m_{1,a}, n_{1,a}) = (1, 0)$. Without loss of generality, we focus on the case $(m_{1,a}, n_{1,a}) = (1, 0)$, since similar arguments hold for the complementary case $(m_{1,a}, n_{1,a}) = (0, 1)$ due to the binary symmetry.

The a -th component of the vector identity Eq. (B2) then reads as

$$1 + m_{2,a} + m_{3,a} = n_{2,a} + n_{3,a}. \quad (\text{B4})$$

Among $m_{2,a}, m_{3,a}, n_{2,a}, n_{3,a} \in \{0, 1\}$, this equation is

solved only by the following choices:

$$(m_{2,a}, m_{3,a}, n_{2,a}, n_{3,a}) = \begin{cases} (0, 0, 1, 0) \\ (0, 0, 0, 1) \\ (1, 0, 1, 1) \\ (0, 1, 1, 1) \end{cases}. \quad (\text{B5})$$

Then once again taking the a -th column of Eq. (B1), observe that the first two cases imply $\vec{m}_1 = \vec{n}_2$ and $\vec{m}_1 = \vec{n}_3$, respectively. Either way, we can again reduce to the case $d = 2$.

Then it remains only to consider the last two cases in Eq. (B5). Taking the a -th column of Eq. (B1), these two cases imply that $\vec{m}_1 + \vec{m}_2 = \vec{n}_2 + \vec{n}_3$ and $\vec{m}_1 + \vec{m}_3 = \vec{n}_2 + \vec{n}_3$, respectively. But then by Eq. (B2), we must have either or $\vec{m}_3 = \vec{n}_1$ or $\vec{m}_2 = \vec{n}_1$, respectively. Either way, we can finally once again reduce to the case $d = 2$, and the proof is complete.

We remark that these combinatorial arguments do not hold when $d \geq 4$ because the list of cases analogous to Eq. (B5) fails to allow us to reduce to the cases $d \leq 3$. \square

-
- [1] P. Hayden, D. Leung, P. W. Shor, and A. Winter, *Communications in Mathematical Physics* **250**, 371 (2004).
- [2] C. Dankert, R. Cleve, J. Emerson, and E. Livine, *Phys. Rev. A* **80**, 012304 (2009).
- [3] H.-Y. Huang, R. Kueng, and J. Preskill, *Nature Physics* **16**, 1050 (2020).
- [4] A. A. Mele, *Quantum* **8**, 1340 (2024).
- [5] Y. Nakata and M. Muraio, *International Journal of Quantum Information* **11**, 1350062 (2013).
- [6] Y. Nakata, M. Koashi, and M. Muraio, *New Journal of Physics* **16**, 053043 (2014).
- [7] P. Aliferis, F. Brito, D. P. DiVincenzo, J. Preskill, M. Steffen, and B. M. Terhal, *New Journal of Physics* **11**, 013061 (2009).
- [8] H.-Y. Hu and Y.-Z. You, *Phys. Rev. Res.* **4**, 013054 (2022).
- [9] M. C. Tran, D. K. Mark, W. W. Ho, and S. Choi, *Phys. Rev. X* **13**, 011049 (2023).
- [10] M. McGinley and M. Fava, *Phys. Rev. Lett.* **131**, 160601 (2023).
- [11] Z. Liu, Z. Hao, and H.-Y. Hu, (2024), <https://doi.org/10.48550/arXiv.2311.00695>.
- [12] D. Gross, K. Audenaert, and J. Eisert, *Journal of Mathematical Physics* **48**, 052104 (2007).
- [13] A. W. Harrow, A. Hassidim, and S. Lloyd, *Phys. Rev. Lett.* **103**, 150502 (2009).
- [14] A. Girard, *Numerische Mathematik* **56**, 1 (1989).
- [15] M. Hutchinson, *Communications in Statistics - Simulation and Computation* **19**, 433 (1990).
- [16] T. Iitaka and T. Ebisuzaki, *Phys. Rev. E* **69**, 057701 (2004).
- [17] E. Knill and R. Laflamme, *Phys. Rev. Lett.* **81**, 5672 (1998).
- [18] R. Cleve, D. Leung, L. Liu, and C. Wang, *Quantum Info. Comput.* **16**, 721–756 (2016).
- [19] R. V. Mishmash, T. P. Gujarati, M. Motta, H. Zhai, G. K.-L. Chan, and A. Mezzacapo, *Journal of Chemical Theory and Computation* **19**, 3194 (2023), pMID: 37227024.
- [20] J. Spencer, *Journal of Combinatorial Theory* **5**, 1 (1968).
- [21] E. F. Assmus and J. D. Key, *Designs and their Codes*, Cambridge Tracts in Mathematics (Cambridge University Press, 1992).
- [22] T. Feder and C. S. Subi (2012).
- [23] H. Bernien, S. Schwartz, A. Keesling, H. Levine, A. Omran, H. Pichler, S. Choi, A. S. Zibrov, M. Endres, M. Greiner, V. Vuletić, and M. D. Lukin, *Nature* **551**, 579 (2017).
- [24] D. Bluvstein, H. Levine, G. Semeghini, T. T. Wang, S. Ebadi, M. Kalinowski, A. Keesling, N. Maskara, H. Pichler, M. Greiner, V. Vuletić, and M. D. Lukin, *Nature* **604**, 451 (2022).
- [25] Z. Baranyai, *Infinite and finite sets* (1974).
- [26] *Topics in Chromatic Graph Theory*, Encyclopedia of Mathematics and its Applications (Cambridge University Press, 2015).
- [27] B. Alspach, J.-C. Bermond, and D. Sotteau, “Decomposition into cycles i: Hamilton decompositions,” in *Cycles and Rays* (Springer Netherlands, Dordrecht, 1990) pp. 9–18.
- [28] R. Glebov, Z. Luria, and B. Sudakov, *Israel Journal of Mathematics* **222**, 91 (2017).
- [29] A. Galicia, B. Ramon, E. Solano, and M. Sanz, *Phys. Rev. Res.* **2**, 033103 (2020).
- [30] S. Sidon, *Mathematische Annalen* **106**, 536 (1932).
- [31] S. W. Golomb, *Academic Press, New York* **23**, 37 (1972).
- [32] K. Drakakis, *Advances in Mathematics of Communications* **3**, 235 (2009).